Sediment transport in mountain rivers

Christophe Ancey[1], Patricio Bohorquez[2], and Eric Bardou[3]

[1] *EPFL, Lausanne, Switzerland*
[2] *CEACTierra, University of Jaén, Spain*
[3] *CREALP, Sion, Switzerland*

Abstract

The paper reviews our recent attempts at modelling bed load transport in mountain rivers. This is a longstanding issue that has attracted considerable attention over the last century. While a number of field and laboratory studies have been instrumental in getting the big picture, there is a clear lack of efficient methods for predicting bed evolution and particle flux. Most approaches to bed load transport have emphasized the existence of a one-to-one relationship between the particle flux and water discharge, but this result conflicts with the spread of data, which often spans over several orders of magnitude.

A possible interpretation lies in the significance of the fluctuations of the particle flux together with the propagation of bed forms. We have therefore developed a theoretical model based on birth-death Markov processes to describe the random exchanges between the stream and bed, which then allows us to derive a governing equation for the particle flux fluctuations. We end up with the probability distribution function of the sediment transport rate. A striking feature is the existence of large fluctuations even under steady flow conditions.

Numerical simulations have been carried out to compute the flow features, for the moment with no sediment transport. These simulations have shown that the kinematic wave approximation (which leads to a significant simplification of the Saint-Venant equation into a nonlinear advection equation) performs well for a wide range of water discharges. Remarkably, it has been found that under steady flow conditions, the local flow variables (wetted section and water discharge, or flow depth and mean velocity) exhibit a Froude similarity, i.e. regardless of the water discharge, the Froude number remains fairly constant at a given place of the river. Future work will consider the inclusion of a stochastic sediment transport equation in the Saint-Venant equations.

1 Introduction

The objective of this paper is to present an innovative approach to sediment transport. The work is done within the framework of a joint project involving EPFL, a research institute of the Wallis canton CREALP, and the University of Jaén (Spain). This project aims to provide a better quantitative picture of sediment transport in gravel-bed rivers, with a particular focus on mountain rivers.

In spite of decades of research, sediment transport, in particular in gravel-bed rivers, is still a difficult issue. For instance, Figure (1) shows the bed load transport rates measured in the Navisence River in Zinal from 2011 to 2013 (1-min averaged flux rates) and the empirical trend given by Meunier's bed load rating curve, which relates the bed load transport rate Q_s (in kg/s) to the water discharge Q_w (in m^3/s) and bed slope i as follows: $Q_s = 9450 i^2 Q_w$ [1]. More sophisticated equations lead to similar or larger errors. At low flow rates, the deviation between the empirical equation and measurements exceeds three orders of magnitude and even at the highest transport rates (for the 8 Aug. 2013 flood, the period of return was ~ 50 yr), there is a conspicuous deviation. This example shows how poor our predictive capacity of bed load transport rate is when empirical equations are used.

This shortcoming has been known for ages although most textbooks on the topic barely mention the tremendous uncertainty associated with bed load transport equations (not to mention the systematic use of log-log plots that minimize the perception of errors and deviations). Each generation of scientists has tackled this issue by arguing that more physics is needed to properly address the problem at hand.

In the 1950s, Hans Einstein proposed a model of bed load transport in which transport results from the difference between the entrainment and deposition rates, E and D, respectively, which depend on the flow conditions and bed geometry [2]. This amounts to writing that on a small interval Δx, the particle flux variation is $\delta q_s = (E-D)\Delta x$, and so the particle flux at bed equilibrium is the implicit solution to the equation $E = D$. The originality of Einstein's treatment lies in the introduction of probabilistic concepts to quantify the probability of entrainment of one particle lying on the bed.

In the 1960s, Ralph Bagnold considered sediment transport as the result of momentum transfers between solid and liquid phases [3]. Bed load transport is essentially a two-phase flow whose dynamics are controlled by the momentum transfers between the water and solid phases.

Needless to say that after decades of investigations, the debate is still open. To advance our understanding of sediment transport, we need to identify the blackspots when building theories of sediment transport. In this paper, we present some of the major difficulties in the current developments. We also refer the reader to recent review papers, which give an comprehensive summary of the state of the art regarding steep gravel-bed rivers, e.g [4]. We then outline a theoretical approach under construction, whose originality lies in its capacity to calculate not only the mean particle flux, but also its probability distribution. We do not claim that this approach solves all of the problems. In fact, laboratory experiments have just provided the proof of concept. Applications to the field require substantial adaptations of the theoretical framework, which is too idealized to be of practical interest (e.g., particles are spherical and of identical size in the current version of the model). Yet, this approach has the potential to elucidate a number of issues arising in the study of bed load transport. The last part of the paper concerns the numerical treatment

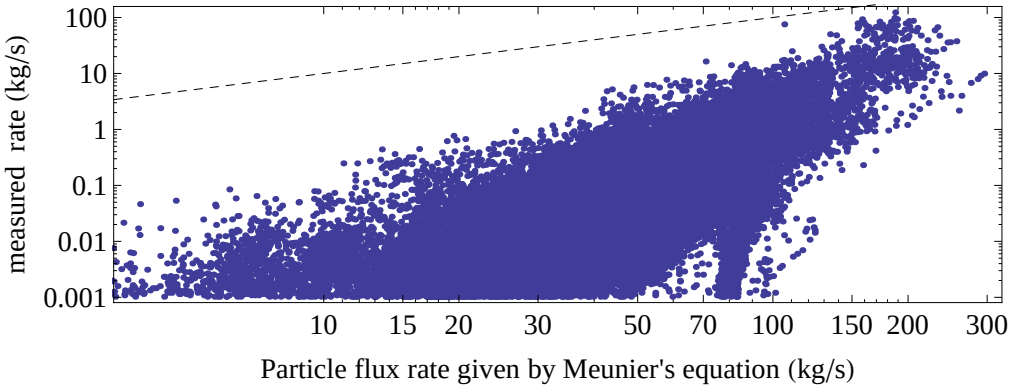

Figure 1: Comparison between bed load transport rates measurements and Meunier's equation for the Navisence river (Zinal, VS). Here the local slope upstream of the station is $i = 3.2\%$.

of the water flow. This is achieved within the framework of the Saint-Venant equations. Here we present the numerical framework and results related to water flow (with no sediment transport). The coupling between the water stream and bed leads to a multitude of challenges that go beyond the scope of this paper. These challenges include the theoretical stochastic framework, which has to be extended to deal with non-uniform flow conditions, and the formulation and numerical resolution of a stochastic Exner equation.

2 Scientific and technical hurdles

This year marks the 100 years anniversary of the report by Gilbert (1914), which is credited with the first comprehensive experimental investigation into bed load transport in inclined flumes [5]. Empirical equations were proposed earlier than Gilbert. For instance, from his observations of the Rhone River south to Tournon (France) in 1879, the French civil engineer Paul du Boys introduced a bed load transport equation from consideration of the bottom shear stress on a granular bed [6]. An analysis of the current literature on bed load transport models shows that there has been no major breakthrough between the earlier attempts by Gilbert or du Boys and the models still used by scientists and engineers today. This does not mean that the state of art is mature (and thus progress is incremental), but on the opposite, there are still many problems to sort out before a new generation of models can be proposed. In this section, we review of the major obstacles to quantitative description of bed load transport.

2.1 Definition of the sediment transport rate

Surprisingly, there is no unique way to define the sediment transport rate. Randomness, intermittency, and rapid changes in the transport rate measurements raise the problem of a suitable procedure that enables calculation and description of sediment flux for both theoretical and practical purposes. In spite of valuable efforts in recent years to gain insight into this issue, it is still unclear whether the different transport rate equations lead to compatible results in terms of statistical properties [7; 8].

An intuitive definition of the particle transport rate is to regard it as the flux of particles through a cross-section S of unit width:

$$q_s = \int_S \mathbf{u}_p \cdot \mathbf{k} dS, \tag{1}$$

with $\mathbf{u}_p$ the particle velocity field and $\mathbf{k}$ the unit normal to S. This definition is rarely used in practice as it is more suited to continuous fields than discrete elements. Therefore, different forms of the sediment transport rate have been proposed. They all assume bed load transport at equilibrium or near equilibrium. On average, they may provide the same values, but the statistical properties of q_s are influenced a great deal. Here are three examples.

A variant of Eq. (1) is to count the number of particles that pass through S over a short time increment δt. The main problem is that q_s is a step function, which takes zero values except at the times of arrival of individual particles; the resulting signal is then very noisy.

Another related form is to count the number of particles that arrive up to time t or to integrate q_s over a short period of time. In the laboratory, this is done by weighting the material accumulated in a basket located at the flume outlet while in the field, sediment traps and bed load samplers are used. These techniques do not provide q_s directly, but the sediment volume per unit width $V(t) = \int q_s(t)dt$. In principe, it should be possible to differentiate V to derive q_s, but in practice, fluctuations in the $V(t)$ records make this operation delicate, which explains why sampling time is a key issue when trying to properly evaluate the solid discharge.

The use of tracer stones in gravel-bed rivers has given rise to a third relationship. From the observation that particles can be moving, lying at rest on the bed surface, or buried in the bed, one can define a virtual velocity, which is the time-averaged velocity U_p of a single particle regardless of its state. Only the upper bed layer participates in bed load transport and is therefore termed the *active layer*; the thickness of this layer is L_a. It represents the depth down to which the bed is continuously reworked by fill and scour. Mass conservation then implies that

$$q_s = U_p L_a. \tag{2}$$

This equation has been used for natural rivers and flume experiments. The statistical properties of $q_s(t)$ depend on the fluctuations of U_p and L_a, which are little known in practice.

So what can we do? From a theoretical perspective, more suitable definitions of the particle transport rate can be borrowed from microstructural models used in

the rheology of particle suspensions. Yet, these models rely on ensemble averages, which lead to numerous difficulties in the calculations or in practical applications. To make the problem more tractable, we can substitute ensemble averages with volume averages. This makes sense when the entire flow is homogeneous, i.e., when the particles are homogeneously distributed in the streamwise direction. For two-phase flows over mobile beds, bed forms usually affect the distribution of moving particles, which makes the assumption of homogeneity dubious. One solution is to introduce a local particle transport rate defined on a control volume ($\mathcal{V} = L \times S$) of length L [9; 10]

$$\bar{q}_s = \frac{S}{V}\sum_{i=1}^{N} u_i v_p = \frac{v_p}{L}\sum_{i=1}^{N} u_i, \qquad (3)$$

where v_p is the particle volume (per unit width) and $u_i = \mathbf{u}_p \cdot \mathbf{k}$ denotes the streamwise velocity component of particle i. Like the *representative elementary volume* in microstructural theories, the control volume must be sufficiently long to contain a number of particles, but short enough compared to the scale of variation of $\bar{q}_s$ on the macroscopic scale.

The introduction of a finite-size volume in Eq. (3) leads to additional problems: how can we distinguish fluctuations that are intrinsic to the phenomenon and those that are induced by the average process? To illustrate this issue, let us consider that we would like to calculate the solids fraction of an ordered packing of cylinders by taking the average over a control volume of length L. See Figure (2). Volume-averaged solids fractions can be calculated as a function of L. When $L \to 0$, we get $\bar{\phi} \to 1$ while for $L \to \infty$, $\bar{\phi} \to \pi/4$. Although there is no randomness in the particle arrangement, the volume-averaged solids fraction exhibits fluctuations, whose amplitude decreases with increasing L as $2\pi a/L$. This clearly shows in that case that the observed fluctuations of $\bar{\phi}$ are not intrinsic, but depend on the control volume. For more complicated situations, e.g. with random particle arrangements, it is more complicated to untangle intrinsic and induced fluctuations. The problem is made even more intricate owing to other processes such as the propagation of bed forms, whose typical length often matches that used for defining the control volume.

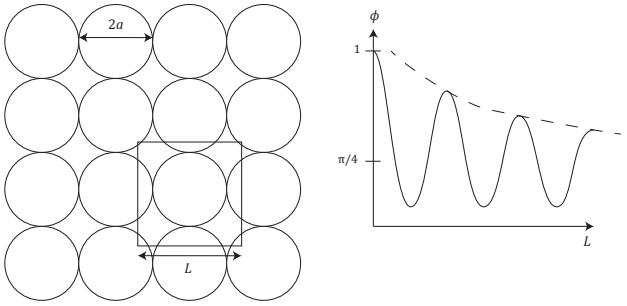

Figure 2: Calculation of the volume-averaged solids fraction.

2.2 Bed structures

A major challenge in fluid mechanics is to understand the origins and mechanisms that lead to the formation of macroscopic structures in systems characterized by apparent disorder. Waterways do not escape the rule. They offer a wide range of bed morphologies exhibiting regular patterns depending on the grain size distribution, bed slope, water flow rate, etc. [11; 12]. Planform structures (e.g., bars and meanders) as well as bed forms (e.g, ripples, dunes, steps and pools) have attracted considerable attention from geomorphologists and hydraulicians. Figure (3) shows the upper reach of the Navisence River at Zinal (Wallis, Switzerland), whose main channel can split into two arms or more (braiding) and exhibits significant sinuosity.

Figure 3: View of the upper reach of the Navisence River, with the stream wandering through its alluvium. The longitudinal profile is given in Figure (11).

A remarkable feature of bed structures is that they emerge quite rapidly at fairly low discharge rates [13]. During intense floods, most bed structures are destroyed and sediment transport occurs in the form of thick layers of grains, a mode of transport called *hyperconcentrated flow* [14]. In many practical situations, gravel beds exhibit undulations, which evolve permanently. Bed structures are thus more the rule than the exception. This is, however, poorly addressed in most laboratory experiments used to derive bed load equations.

The mainstream view is that that bed structures arise from a loss of stability of the bed due to the coupling between the turbulent water stream, sediment transport, and bed topography [15]. The main difficulty is that depth-averaged equations such as the Saint-Venant-Exner equations (see § 3.1) are linearly stable for Froude numbers as large as 2. The calculation of bed form initiation and propagation then requires a more elaborate framework [16].

An alternative approach to pattern formation highlights the part played by random fluctuations of the particle transport rate q_s in the development of bed forms [17]. Analogies can be drawn with many nonlinear physical systems, in which fluctuations can produce spatially regular structures as a result of noise-induced transitions between different states of the system [18]. In the absence of a more fundamental understanding of bed load transport fluctuations, the simplest idea has been to add a noise term to the governing equations. For instance, Jerolmack and Mohrig showed that the growth and steady-state dimensions of sand dunes can be successfully captured using white noise in the Exner equation [19].

Regardless of the precise mechanism that rules their dynamics, it is clear that bed structures markedly affect the water flow, which in turn influences bed form initiation and propagation. Field surveys, laboratory experiments and numerical simulations have provided clear evidence that flow resistance is controlled to a large extent by bed forms [20]. For instance, in the absence of bed

forms, there is a one-to-one smooth relationship between the water discharge q and flow depth h, but when these bed forms develop, this relationship exhibits a more complicated pattern (non-uniqueness, hysteretic behaviour). Bedforms are also often regarded as the main source of particle flux fluctuations [21; 22; 23]: for instance, as bed slope is locally quite different between the stoss and lee sides of dunes, there is a significant change in the water flow conditions (thus particle transport) and particle entrainment.

2.3 Separation of scales

The advent of modern science is tightly tied to the *reductionist* approach (i.e., any system can broken down into individual elements, whose understanding helps us to get to grips with the whole system) [24]. Part of the success of this approach lies in the separation of length and time scales for many problems. For instance, for monoatomic gases, starting from the description of collisions at the particle scale (kinetic theory), we can derive macroscopic equations of conservation (Navier-Stokes equations) on the macroscopic scale. In that case, the large difference between the atom size and the typical length scale of continuum mechanics makes it possible to treat each problem separately. The linkage between the micro- and macro-descriptions is ensured through averaging. This procedure works at coarser scales (typical examples in computational fluid mechanics include large eddy simulations, in which averaging is replaced by low-pass filtering).

A hierarchical decomposition of the fluvial system into nested components (from watershed to particle) has been proposed [11], but a striking detail of the decomposition is the overlap of scales and the varying nature of the elements involved: while for Newtonian fluids, there is a clear separation between the molecular scale, Kolmogorov' microscales of turbulence, and flow length scale, it is no longer the case for instance, between bed components such as boulders and the flow depth (mountain streams are mostly characterized by low submergence, i.e. the flow depth is just a few times larger than the typical bed roughness). Figure (4) shows the Navisence River upstream of the measurement station: the typical flow depth is 50 cm while the mean diameter is $d_{50} = 10$ cm. Note also the presence of vegetation, which plays a role often overlooked, e.g., jamming wood debris during floods [25] and consolidating effects of root systems on the long run [26].

Figure 4: View of the Navisence River near the measurement station of Zinal.

2.4 Particular realization vs. mean trend

Field surveys have shown that the sediment transport rate seems to closely follow the time variations in the water discharge. Figure (5) shows a typical example of evolution for the Navisence River. In this mountain stream, sediment transport is highly intermittent: it occurs primarily in spring and summer as a result of snowmelt, glacier runoff, and rainstorms, and tapers off during the cold season. Yet, as shown by Figure (4), there is no one-to-one relationship between the water discharge and sediment transport rate: for a given water discharge, the sediment flux spans often over two to three orders of magnitude, which shows that under similar flow conditions, the actual sediment flux can be quite different from the mean trend. This spread of data has significant implications. First, most theoretical models are only concerned with mean fluxes and so, it is extremely difficult to test models against field and laboratory data when these data span over several orders of magnitude. Then, in many practical applications, focus is on different variables related to sediment transport. For instance, for calculating the time associated with reservoir filling, one is interested in determining the volume of sediment as a function of time. Owing to the random variation of the sediment flux, this volume is a stochastic integral. The actual value of the sediment volume at a given time is also quite different from the mean trend $V(t) = \int Q_s dt$. Strikingly, most—if not all—models developed so far ignore this problem of bed load transport variability whereas it should be at the heart of the concerns.

3 Outline of the theoretical framework

Here we outline the model under development. In the construction of this model we have tried to tackle the different issues presented in § 2. To date, we have essentially focused on the determination of the particle transport rate. The water phase is assumed to be properly described using the Saint-Venant equations (see § 3.1). The coupling between bed load transport and water flow is achieved primarily through the Exner equation, which expresses the conservation of mass for the bed. This framework implies that turbulence is roughly described by simple scalar relationships (e.g., the Manning-Strickler equation for flow resistance). As turbulence is key in the entrainment of particles from the bed and their subsequent motion, averaged equations such as the Saint-Venant equations may be too crude to capture the flow dynamics in all its various aspects, but in a first stab at modelling sediment transport, we assume that they are sufficient to provide the main features of the water flow. More attention is paid to the Exner equation, which is useful not only to compute the mean particle flux (or more precisely, the gradient of the particle flux), but also particle exchanges between the bed and stream. To that end, we take inspiration from other approaches taken in kinetic chemistry or population dynamics, which lead to evolution equations for the chemical components or the species (see § 3.2). For the particle velocity fluctuations, we use a simple analogy with Brownian motion of particles in a potential to derive the probability distribution function of the particle velocity. We eventually end up with the probability distribution of the particle transport rate.

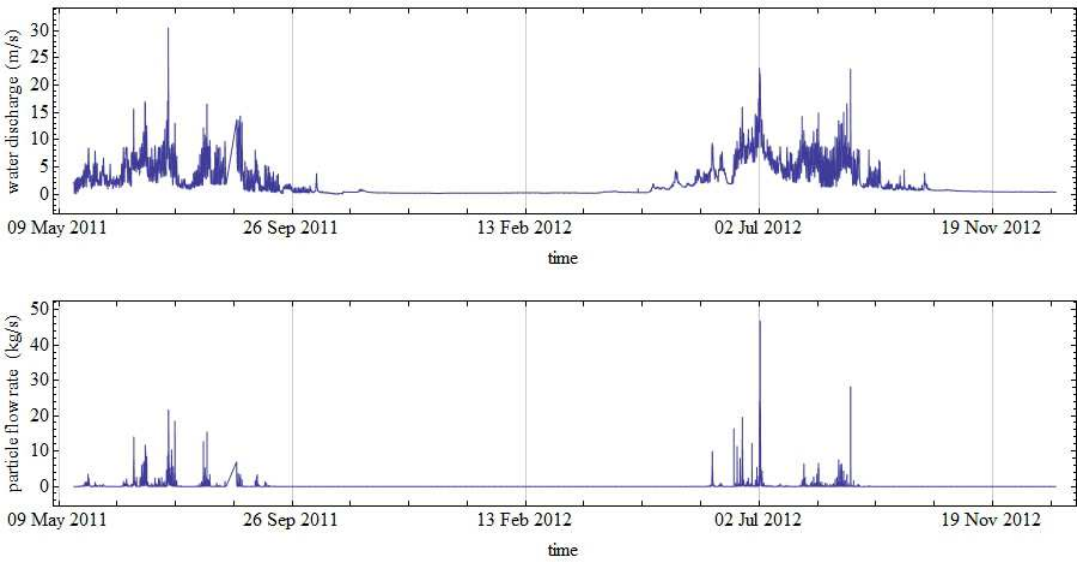

Figure 5: Time series showing the water discharge and the sediment transport rate from May 2011 to Dec. 2012 in the Navisence River, Zinal.

3.1 Saint-Venant-Exner equations

For one-space variable problems, the simplest morphodynamic model comprises the shallow-water (Saint-Venant) equations for the conservation of mass and momentum of the water phase and the Exner equation for the continuity equation of the bed [27]:

$$\frac{\partial h}{\partial t} + \frac{\partial h\bar{v}}{\partial x} = 0, \quad (4)$$

$$\frac{\partial h\bar{v}}{\partial t} + \frac{\partial h\bar{v}^2}{\partial x} + gh\cos\theta\frac{\partial h}{\partial x} = gh\sin\theta - \frac{\tau_b}{\varrho}, \quad (5)$$

$$(1-\zeta_b)\frac{\partial y_b}{\partial t} = -\frac{\partial \bar{q}_s}{\partial x} = D - E, \quad (6)$$

in which $h(x,t) = y_s - y_b$ denotes the flow depth, $y_b(x,t)$ and $y_s(x,t)$ the positions of the bed and free surfaces, $\bar{v}$ the depth-averaged velocity, x the downstream position, t time, ϱ the water density, τ_b is the bottom shear stress, ζ_b the bed porosity, $\bar{q}_s$ the average bed load transport rate, and D and E represent the deposition and entrainment rates, respectively. The bed slope is defined as $\tan\theta = -\partial_x y_b$. In most models based on Eq. (4)–Eq. (6), the governing equations are closed by empirical relationships for the flow resistance τ_b and sediment transport rate $\bar{q}_s$, both being functions of the flow variables $\bar{v}$ and h, and additional parameters (e.g., bed roughness and slope).

Whereas the Saint-Venant equations are classical and their physics is seldom called into question, the coupling with the Exner equation leads to numerous difficulties both physically and mathematically [28; 29]. Several derivations of the Exner equation have been proposed for different situations including variations in sediment properties or changes in the boundary conditions (e.g, tectonic uplift for landscape dynamics problems) [30; 19; 7; 31; 8]. A central theme in all of these derivations is that the Exner model is an averaged equation that specifies the rate of buildup/erosion of the bed surface as a function of the sediment flux through the surfaces defining the control volume over which the averaging has been done. The average sediment transport rate has nontrivial effects on the flow dynamics owing to the strong nonlinearities and coupling in the governing equations Eq. (4)–Eq. (6). Indeed, the sediment flux affects the bed surface $y_b(x,t)$ (thus its slope angle θ) through the Exner equation Eq. (6), and it may also influence flow resistance depending on the empirical parametrization chosen for the bottom shear stress τ_b [32].

Our guess is that, if fluctuations are relevant to the macroscopic description of bed load transport, then the mean-field Exner equation Eq. (6) cannot properly account for the bed evolution or particle flux, or at least, as is the case for algebraic closure equations used in turbulence, this equation is a gross approximation of reality. To clarify this point, we need to take a closer look at the microdynamics of the bed evolution as a result of entrainment and deposition of particles.

3.2 Evolution of the number of moving particle

The idea is to count the number of moving particles in a control volume or in an array of adjacent volumes of length Δx. In each elementary volume, the number of moving particles varies with time as a result of transport and exchanges with the bed (see Figure (6)). We do not discriminate between rolling and saltation and treat both motions as a single species which we call the moving particles. A convenient framework for the investigation of the statistics of these exchanges is the theory of birth-death Markov processes, widely used in population-dynamics models or chemical kinetics [33].

As for any idealized formulation, a tradeoff between physical scope and mathematical tractability has had to be found. To achieve analytical results, we introduce a number of simplifications:

- The sediment comprises spherical particles of equal diameter d and density ϱ_p.
- We consider a two-dimensional steady water stream flowing down a sloping bed composed of particles identical to those transported. The bed breadth B is assumed to be indefinitely large.
- The water flow is characterized by its depth-averaged velocity $\bar{v}(x,t)$ and flow depth $h(x,t)$, which are assumed to be prescribed and independent of the sediment transport. The water flow is

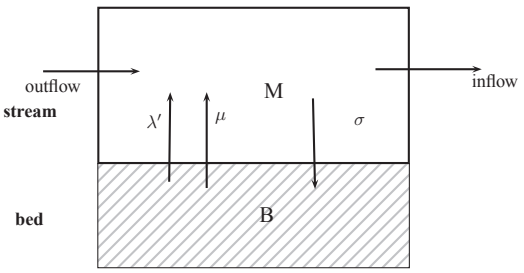

Figure 6: Sketch showing the processes considered for calculating the evolution of the number N of moving particles M within an observation window of length Δx. This number can be increased when particles enter the volume or are entrained as a result of individual and collective entrainments from the bed B (with a respective rate λ' and μ); N decreases when particles leave the volume or are deposited (with a rate σ).

turbulent, but the details of the turbulence and velocity field are ignored. Turbulence dissipation and flow resistance due to the particles are entirely encoded in the $\tau_b(\bar{v}, h)$ expression, which will not be studied here.

- The concentration of moving particles is small and so particle interactions may be neglected. In terms of the bed load transport regime, this also means that the bed shear stress narrowly exceeds the threshold for incipient sediment motion.

- The water stream drives the sediment phase: the particle phase is subordinate to the water phase in that the mean particle velocity $\bar{u}_s$ is controlled by the water flow conditions, but due to particle exchanges (entrainment/deposition) between the bed and stream as well as particle velocity fluctuations, the instantaneous particle flux q_s undergoes variations of different magnitudes.

- The bed is initially flat and here we do not consider the development of bed forms, even though after a finite time such bed forms are likely to develop and affect water flow and sediment transport.

- We assume that the number of particles making up the bed is infinite, i.e., whenever a particle at the bed interface is set in motion, the shape of the interface is altered, but not the number of particles available to entrainment at the bed interface.

- As we study steady uniform flows over flat beds (free of patterns), we do not address the dependence of the model coefficients on the Shields stress or any other parameterization of the flow conditions. These coefficients (e.g., entrainment and deposition rate coefficient) are thus constant in the following developments. Note that the final structure of the governing equations will not be affected by this assumption.

If there are N moving particles within the control window, the probability of deposition within the time increment δt is $\sigma N \delta t$, with σ the deposition rate. For entrainment, we assume that there are two processes referred to as individual and collective entrainment resulting in a probability of entrainment $P = (\lambda' + \mu N)\delta t$, where λ' and μ denote the individual and collective entrainment rates, respectively. *Collective entrainment* acts as a feedback loop: as will be shown later, μ is a key parameter, which controls the development and strength of wide fluctuations. A caveat is in order: here, *collective entrainment* implies that the probability of entrainment depends not only on the flow conditions (through λ'), but also on the number of moving particles (through μ) as these can impact the bed and impart momentum to the bed particles, favouring their entrainment. In contrast with the physics of phase transition, it does not involve the existence of long-range correlations. It does not mean that there are massive departures of particles (avalanches) within short time spans. For subsequent use, we also introduce a volumetric particle entrainment rate per unit length $\lambda = \lambda' \varpi_p / \Delta x$ and the differential rate $\kappa = \sigma - \mu$ between deposition and collective entrainment.

The evolution of the number of moving particles could be described using the following forward master equation:

$$\begin{aligned} \frac{\partial}{\partial t} P_n(n,t) &= (n+1)\sigma P_n(n+1,t) \\ &\quad + (\lambda' + (n-1)\mu)\, P_n(n-1,t) \\ &\quad - (\lambda' + n(\sigma+\mu))\, P_n(n,t). \end{aligned} \tag{7}$$

Steady-state solutions to this equation can be obtained using the probability generating function. A stumbling block in this approach is that the governing equation for N involves discrete probabilities. To generalize the model and derive a continuum formulation, we wish to replace the discrete variable N with a continuous variable. A classical strategy is to introduce the density number $c = N/\Delta x$. The governing equation for the density number can be obtained from Eq. (7) by using the Kramers-Moyal or system-size expansion. This technique was used in a former paper [7]. The problem is that the resulting governing equation involves an infinite series of terms. Even if the objective is to find an approximation of the probability distribution, the number of terms required in the truncated series increases significantly when $\Delta x \to 0$, which makes the analytical approximation of little interest.

Exact solutions can be determined by using the equivalent of a Fourier transform, called the Poisson representation [34]

$$P(n,t) = \int_{\mathcal{C}} \frac{e^{-a} a^n}{n!} f(a,t) da, \tag{8}$$

where integration is made over a certain domain $\mathcal{C}$ and $f(a,t)$ is a positive real-valued function. Fourier transforms are reversible operations that map the time and frequency domains in spectral theory of signals. On many occasions when working with times series, it is easier to work in the frequency domain than the original time domain. Similarly here, the Poisson transform can be introduced to map the discrete and continuous probability domains. Using this transform, we have shown that the master equation Eq. (7) can be transformed into a second-order nonlinear parabolic diffusion equation, which has the same structure as that of a Fokker-Planck equation

$$\frac{\partial f}{\partial t} = \mu \frac{\partial^2 a f}{\partial a^2} - \frac{\partial}{\partial a}[(\lambda' - a(\sigma - \mu))f], \tag{9}$$

with $f(a)$ the transform of P in the a-space. This equation also arises in economics to model short-term interest rates [35].

The decisive advantage of this formulation is that we can readily obtain exact solutions in the a-space for

steady-state or time-dependent flow conditions. Further information such as the autocorrelation function and moments can also be derived straightforwardly. Algorithms simulating the process are also available to study time-dependent flow problems [36].

This formulation has, however, disadvantages: while analytical calculations are easier in the a-space, it is difficult to return to the physical variables. As a consequence, if we are able to compute the probability density function f in the a-space or to provide its governing equation, the back-transformation is uneasy. It is possible to relate the moments of f and N, but hardly possible to provide more information on the stochastic variation of N, which hinders, for the moment, the development of a stochastic Exner equation.

Under steady state conditions and in the absence of bed forms, it is possible to calculate the probability of finding n moving particles within the control volume. When the collective entrainment μ is nonzero, the solution to Eq. (7) is the negative binomial distribution

$$P_s(n) = \mathrm{NegBin}(n; r_{nb}, p) = \frac{\Gamma(r+n)}{\Gamma(r_{nb})n!} p^{r_{nb}}(1-p)^n, \quad (10)$$

with $r_{nb} = \lambda'/\mu$ and $p = 1 - \mu/\sigma$, and where Γ denotes the gamma function. The mean is

$$\langle N \rangle = \frac{\lambda'}{\sigma - \mu}, \quad (11)$$

and the variance is

$$\mathrm{var}\, N = \frac{\lambda'\sigma}{(\sigma-\mu)^2}. \quad (12)$$

For $\mu = 0$, we obtain the Poisson distribution of rate $r_p = \lambda'/\sigma$,

$$P_s(n) = \frac{(r_p)^n}{n!} \mathrm{e}^{-r_p}, \quad n = 0, 1, \ldots. \quad (13)$$

3.3 Velocity fluctuations

Many models have been proposed to compute the mean particle velocity, but the probability distribution of the velocity for a single particle has not been well investitive until very recently [37; 38; 39; 40]. We have developed a very simple model, in which, making the analogy with Brownian particles in a potential, we end up with the probability distribution in the form of a truncated Gaussian distribution:

$$P_u^{eq}(u) = \sqrt{\frac{2t_r}{\pi D_u}} F(u), \quad (14)$$

with

$$F(u) = \frac{\exp\left(-\dfrac{t_r(u-\bar{u}_s)^2}{2D_u}\right)}{1 + \mathrm{erf}(\bar{u}_s\sqrt{t_r}/\sqrt{2D_u})} \quad (15)$$

where t_r is a relaxation time, D_u is the equivalent of a particle diffusivity, and $\bar{u}_s$ is the mean particle velocity imposed by the water stream, i.e. the asymptotic value to which the particle velocity tends at long times in the absence of fluctuations.

We tested Eq. (14) against experimental data. The detail can be found in an earlier paper [10]. The bed was composed of gravel characterized by a narrow size distribution around a mean diameter 8 mm. The particle density was 2650 kg m^{-3}. Particle motion was tracked using a high-speed camera over a 40 cm length. Figure (7) shows the probability density function of the particle velocity up computed from 755 trajectories. The flow conditions were the following: depth-averaged velocity of water $\bar{v} = 92.5$ cm s^{-1}, mean flow depth $h = 2$ cm, Froude number Fr $= 2.1$, flow Reynolds number Re $= 18\times10^3$, Shields number Sh $= \varrho h \sin\theta/[(\varrho_p - \varrho)d] = 0.042$. For these flow conditions, long wavelength bed forms developed.

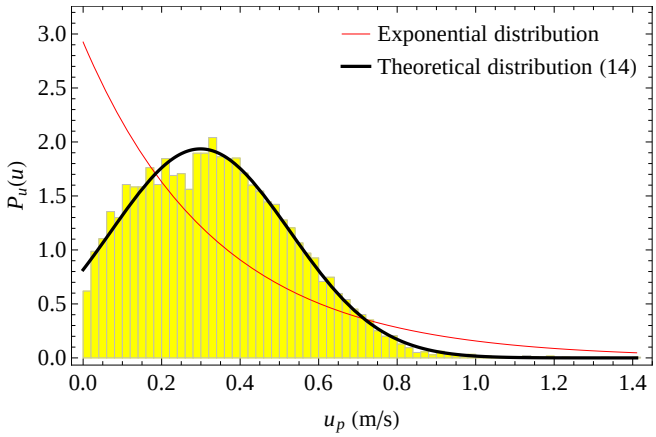

Figure 7: Probability distribution for the particle velocity. The histogram represents the empirical probability density function of u_p. The thick black solid line is the theoretical distribution Eq. (14) with $\bar{u}_s = 29.9$ cm s^{-1} and $\zeta = 5.7$. The thin red line shows the exponential probability distribution $P_u(u) = \mathrm{e}^{-u/\bar{u}_s}/\bar{u}_s$, still with $\bar{u}_s = 29.9$ cm s^{-1}. The dimensionless parameter ζ is defined as $\zeta = \bar{u}_s/\sqrt{D_u/t_r}$.

There is a fairly good agreement between these data and the truncated Gaussian distribution Eq. (14). This result compares well with the observations made by Martin *et al.* [38] with similar flow conditions. Our results contrast with those obtained by Fan *et al.* [40], Robeseberry *et al.* [41], and Lajeunesse *et al.* [37], who found that the empirical probability distribution of particle velocity u_p was well captured by an exponential distribution. This discrepancy may originate from the differences in the experimental set-up.

Although there is experimental evidence for the theoretical velocity distribution Eq. (14), the diversity of experimental data shows that its range of application is unlikely to cover all sediment sizes. We note, however, that in either case, the truncated Gaussian and exponential laws are thin-tailed, a result that can be anticipated as it is uncommon for the highest particle velocities to exceed fluid velocities. Therefore, the high fluctuations of sediment transport rates are unlikely to stem from a thick tail of the velocity distribution.

3.4 Particle flux fluctuations

As a matter of convenience, we express the instantaneous particle flux as the number of moving particles per unit time within the control volume rather than their volume

$$\dot{n}(t; \mathcal{V}) = \frac{1}{\Delta x} \sum_{i=1}^{N(t)} U_{p,i}, \quad (16)$$

where both N and $U_{p,i}$ are random variables. For a stationary process, their probability distributions are given by Eq. (10)—or Eq. (13) if $\mu = 0$—and Eq. (14), respectively. The probability density function of the sum of

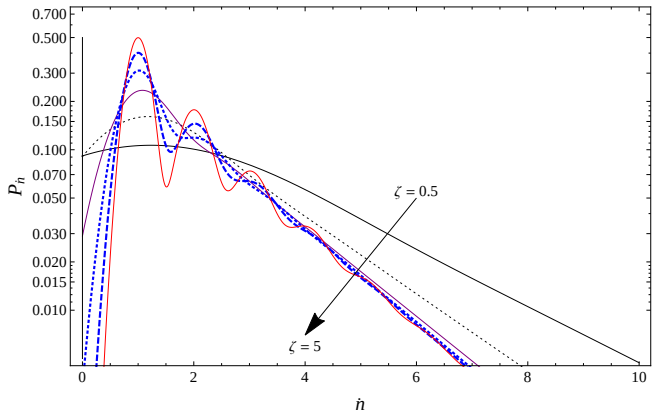

Figure 8: Shape of the probability density function $P_{\dot{n}}(\dot{n})$ given by Eq. (17) in a log-linear plot for different values of ζ (the arrow shows increasing ζ values): $\zeta = 0.5$ (black solid line), $\zeta = 1$ (black dotted line), $\zeta = 2$ (purple solid line), $\zeta = 3$ (blue dotted line), $\zeta = 4$ (blue dashed line), and $\zeta = 5$ (red solid line). All of the other parameters are kept constant: $\Delta x = 1$ m, $\bar{u}_s = 1$ m s^{-1}, $r = 1$ ($\lambda' = \mu$) and $p = 0.5$ ($\sigma = 2\lambda'$). The mean particle flux $\langle \dot{n} \rangle$ is 1.541, 1.115, 1.007, 1.000, 1.000, 1.000 beads s^{-1} when ζ is increased from 0.5 to 5. The square coefficient of variation $\mathrm{var}\, \dot{n}/\langle \dot{n} \rangle^2$ is 2.410, 2.362, 2.209, 2.109, 2.062, and 2.040 beads^2 s^{-2} when ζ is increased from 0.5 to 5.

random variables drawn from the same distribution can be calculated by taking the Fourier transform of the convolution product, then inverting the result. After a little bit of work, we eventually find that

$$P_{\dot{n}}(\dot{n}) = P_s(0)\delta(\dot{n}) + \frac{\zeta \Delta x}{\bar{u}_s}\sqrt{\frac{2}{\pi}}\sum_{k=1}^{\infty} P_s(k) G(\dot{n}), \qquad (17)$$

with

$$G(\dot{n}) = \frac{\exp\left[-\zeta^2 \dfrac{(\dot{n}\Delta x - k\bar{u}_s)^2}{2k\bar{u}_s^2}\right]}{\sqrt{k}(1 + \mathrm{erf}(\sqrt{k}\zeta/\sqrt{2}))} \qquad (18)$$

where $P_s(k)$ is given by Eq. (10) if $\mu > 0$ and Eq. (13) if $\mu = 0$. We have also introduced the dimensionless number $\bar{u}_s/\sqrt{D_u/t_r}$. The probability density function of $\dot{n}$ is discontinuous at $\dot{n} = 0$: there is a finite probability $P_s(0) = (1 - \mu/\sigma)^{\lambda'/\mu}$ for $\mu > 0$ ($P_s(0) = \exp(-\lambda'/\sigma)$ for $\mu = 0$) that there is no moving particle within the window, in other words, that the particle flux is zero (intermittent sediment transport).

Some remarkable features can be deduced from numerical evaluations of Eq. (17). Figure (8) shows examples of variations of $P_{\dot{n}}(\dot{n})$ for ζ ranging from 0.5 to 5. For low ζ values, the probability density function varies smoothly and slowly except for the point of discontinuity $\dot{n} = 0$, as explained above. Increasing ζ leads to (i) a faster (but still exponential-like) decay at larger values of $\dot{n}$, which is little influenced by the actual value of ζ, and (ii) the development of sharp peaks of probability for the lowest values of $\dot{n}$: in a dilute flow much of the flux is carried by a couple of particles and, in the absence of velocity fluctuations, the particle flux exhibits this bumpy landscape in which each peak corresponds to the crossing of one particle.

Although Einstein used probabilistic concepts to derive his bed load equation, he did not end up with a probability distribution for the sediment transport rate. His arguments lead to a binomial variation of the number of moving particles, thus a Poisson distribution in the limit $p \to 0$ (i.e. $\mu \to \sigma$) and $N \gg 1$ [2]. This means that intense sediment transport exhibits bounded Poissonian fluctuations, with the coefficient of variation $\mathrm{var}^{1/2}\, q_s/\langle q_s \rangle = r_p^{-1/2}$ given by the steady-state Poisson distribution Eq. (13). Hamamori is credited with the first attempt to derive the probability distribution for the sediment transport rate. He considered that bed load transport rate fluctuations arise from the migration of bed forms [42]. He obtained a nonparametric density distribution function of the bed load transport rate

$$P(q_s) = \frac{1}{4\langle q_s \rangle} \log\left(4\frac{\langle q_s \rangle}{q_s}\right), \qquad (19)$$

which implies that the fluctuations are bounded: $0 < q_s < 4\langle q_s \rangle$, and that the square coefficient of variation is constant: $\mathrm{var}\, q_s/\langle q_s \rangle^2 = 7/9$. More recently, Turowski used a two-parameter distribution derived from the normal distribution, called the Birnbaum-Saunders distribution

$$P(q_s) = \frac{q_s + \alpha}{2\beta q_s \sqrt{2\pi\alpha q_s}} \exp\left[-\frac{(q_s - \alpha)^2}{2\alpha\beta^2 q_s}\right], \qquad (20)$$

with α and β two calibration parameters [43]. The mean value is $\langle q_s \rangle = \alpha(1 + \beta^2/2)$ and the coefficient of variation is found to range from 0 to $\sqrt{5}$. Figure (9) shows the comparison of the probability distributions Eq. (17), Eq. (19), Eq. (20) for a particular case. As the fluctuations are bounded, Hamamori's relation is unable to capture the exponential tail of the distribution and tends to overestimate the bed load transport rate significantly (compared with what Eq. (17) predicts) in the limit of $\dot{n} \to 0$. This latter shortcoming is also observed for the Birnbaum-Saunders distribution, but the tail behaviour is consistent with that predicted by our model Eq. (17). On the whole, the general impression one gets from Figure (8) is that the Birnbaum-Saunders distribution smooths out the ups and downs in the probability distribution Eq. (17). Although the point of this paper is not to discuss the agreement with field and experimental data, note that that high-resolution data confirm (i) the significant proportion of zero values of the particle flux and (ii) the highly fluctuating nature of time series, two features that are consistently described by Eq. (17) and Figure (9) [9; 44; 45].

Comparison with experimental data usually shows a decent agreement between theory and experiment. Systematic comparison was done with an idealized setup, in which sediment was replaced by 6-mm glass beads free to move in a narrow flume [9]. Figure (10) shows the empirical and theoretical probability density functions $P_{\dot{n}}(\dot{n})$ for a slope of 5°. One possible reason for the discrepancy between theory and experiment is the existence of two populations of moving particles with two distinctive mean velocities. Indeed, there is a size factor of about 5 between the velocities in the rolling and saltating regimes. Comparing the different runs also shows that the larger the number of moving particles, the better the agreement. This may be an indication either that theory performs less well in the limit $N \to 0$ or the calculation of the sediment transport rate is biased as we assumed that the probabilities $P_n(n)$ and $P_u(u_p)$ were independent in order to obtain $P_{\dot{n}}(\dot{n})$ by taking the Fourier transform of the convolution product. This requires further work. A more thorough experimental investigation is still needed to test the model.

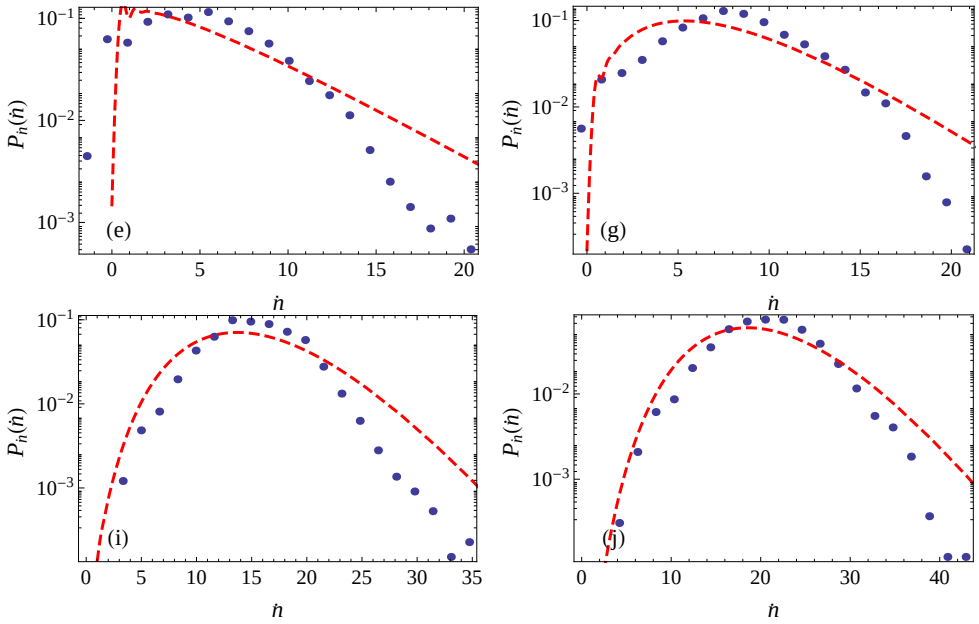

Figure 10: Probability density functions for the particle flux compared to experimental data collected by Tobias Böhm [9]. The dots represent the empirical probability density function while the dashed curves are the theoretical distributions Eq. (17) with $\zeta = 4$. This parameter was fixed arbitrarily, but provided that $\zeta > 3$, we found that altering ζ did not change the shape of $P_{\dot{n}}(\dot{n})$ significantly for these runs. Run (e) $\overline{\dot{n}} = 5.3$ beads/s, $h = 10.2$ mm, $\bar{u}_s = 0.41$ m/s. Run (g) $\overline{\dot{n}} = 8.0$ beads/s, $\bar{u}_s = 0.44$ m/s, $h = 12.2$ mm. Run (i) $\overline{\dot{n}} = 15.4$ beads/s, $h = 16.9$ mm, $\bar{u}_s = 0.48$ m/s. Run (j) $\overline{\dot{n}} = 20.0$ beads/s, $h = 19.4$ mm, $\bar{u}_s = 0.53$ m/s. See [10] for further information.

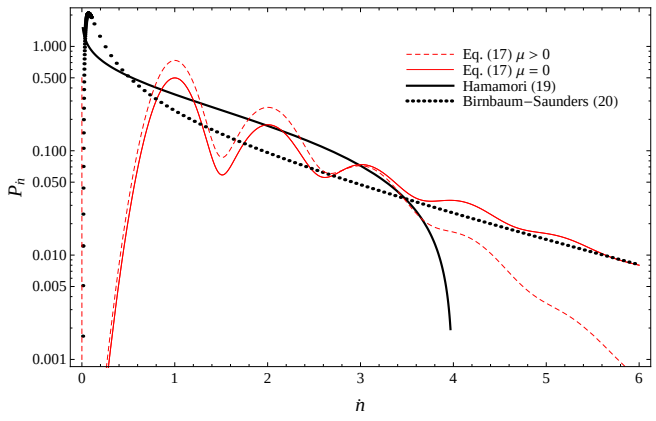

Figure 9: Comparison of the probability density function $P(\dot{n})$ in a log-linear plot: Hamamori's equation Eq. (19) (with $\langle \dot{n} \rangle = 1$ bead s^{-1}) and Birnbaum-Saunders distribution Eq. (20) (with $\alpha = 0.451$ and $\beta = 1.556$). We also report the probability density function $P_{\dot{n}}(\dot{n})$ for $\zeta = 5$ ($\Delta x = 1$ m, $\bar{u}_s = 1$ m s^{-1}): when the number of moving particles follows the negative binomial distribution Eq. (10) (solid red line) with $r = 1$ ($\lambda' = \mu$) and $p = 0.5$ ($\sigma = 2\lambda'$) or the Poisson distribution Eq. (13) (dashed red line) with $r_p = 1$ bead s^{-1}. Except for the Poisson distribution (whose variance equals the mean), the coefficient of variation is $\sqrt{2}$ and all of the distributions have the same mean ($\langle \dot{n} \rangle = 1$ bead s^{-1}).

3.5 Local and macroscopic forms of the Exner equation

The last building block is to make a link between the Exner equation Eq. (6) and the local conservation of mass. By integrating the velocity probability equation, we obtain an equation for the particle concentration or, equivalently, the particle activity (the volume of particles per unit bed length) $\gamma(x,t) = N\varpi_p/\Delta x$

$$\frac{\partial}{\partial t}\langle\gamma(x,t)\rangle + \frac{\partial}{\partial x}(\bar{u}_s\langle\gamma(x,t)\rangle) = \frac{\partial^2}{\partial x^2}(D_u\langle\gamma(x,t)\rangle) + \lambda - \kappa\langle\gamma(x,t)\rangle, \tag{21}$$

with $\kappa = \sigma - \mu$ and $\lambda = \lambda'\varpi_p/\Delta x$. This is a linear advection diffusion equation with a source term. Albeit of very common structure, this equation yields many interesting insights into the physics of sediment transport. Note that Eq. (21) can also be cast in the following form

$$\frac{\partial}{\partial x}\mathcal{Q}(x,t) = E(x,t) - D(x,t) - \frac{\partial}{\partial t}\langle\gamma\rangle, \tag{22}$$

with $\mathcal{Q} = \bar{u}_s\langle\gamma\rangle - \partial_x(D_u\langle\gamma\rangle)$, $E = \lambda + \mu\langle\gamma\rangle$, and $D = \sigma\langle\gamma\rangle$. Interestingly, if we borrow the definition of the sediment flux rate from David Furbish [31] and refer to $\mathcal{Q}$ as the *macroscopic sediment transport rate*, then Eq. (22) is the generalized Exner equation established by a number of authors [46; 47; 30]. Note that the standard equation Eq. (6) does not usually include the time variation in the particle activity $\partial_t\langle\gamma\rangle$ as this term is vanishingly small. Indeed, using dimensional analysis, [48] showed that provided that the ratio $\epsilon = \bar{q}_s/q_w$ (with q_w the water discharge) remains small, the time variation $\partial_t\langle\gamma\rangle$ is second order. Thus to leading order, the bed evolution $\partial_t y_b$ is controlled by the gradient $\partial_x\bar{q}_s$.

The existence of diffusive effects in the Exner equation may lead to the conclusion that by smoothing out

particle activity variations $\langle \gamma(x,t) \rangle$ along the bed, particle fluctuations dissipate short wavelength perturbations and so make the bed more stable. Yet, as exemplified by Turing patterns in certain reaction-diffusion systems [49], diffusion may amplify instabilities instead of dampening them under a slight perturbation by noise.

4 Numerical modelling

In this section we present numerical results to describe the flow hydrodynamics in the upper reach of the gravel bed Navisence river between Mottec and Zinal glacier (5.5 km in length), see Figure (11). The mean bed gradient is 4.1%, which is regarded as steep according to geomorphological criteria, but this mean slope is shallow in the mathematical sense (i.e. $\cos\theta \approx 1$), with the important consequence that the pressure distribution (across the depth) is hydrostatic and the Saint-Venant equations are well-suited.

The river exhibits a rich collection of geomorphological features such as steps and pools sequences, meanders, multi-channels and slosh dynamics that increase flow resistance with respect to regions of quasi-uniform flow because of mechanical losses due to flow expansion/contraction, dead zones and channel geometry variations. This pushes us to use cross sectionally averaged formulations of the Saint-Venant equations as these better accounts for streamwise variations of water flow conditions along the river.

4.1 Cross-sectionally averaged Saint-Venant equations

The one-dimensional version of Saint-Venant equations Eq. (4)-Eq. (6) can be extended to account for cross sectional variations as described by Cunge et al. [50]:

$$\frac{\partial \mathbf{U}}{\partial t} + \frac{\partial \mathbf{F}}{\partial x}(x,\mathbf{U}) = \mathbf{S}(x,\mathbf{U}), \tag{23}$$

with

$$\mathbf{U} = (A, Q)^T, \tag{24}$$

$$\mathbf{F} = \left(Q, \frac{Q^2}{A} + gI_1\right)^T, \tag{25}$$

$$\mathbf{S} = \left[0, gI_2 + gA(S_0 - S_f)\right]^T, \tag{26}$$

in which A is the wetted cross-sectional area and $Q \equiv \bar{v}A$ is the water flow rate. The term I_1 represents a cross-sectional hydrostatic pressure force,

$$I_1(x,A) = \int_0^{h(x,A)} [h(x,A) - \eta]\sigma(x,\eta)d\eta, \tag{27}$$

in which the surface water level is denoted by $h(x,A)$ and the local width $\sigma(x,\eta)$ at a given depth is

$$\sigma(x,\eta) = \frac{\partial A(x,t)}{\partial \eta}, \tag{28}$$

In Eq. (26), I_2 is the component of the pressure force in the main stream direction due to the reaction of the walls arising from shape variations

$$I_2(x,A) = \int_0^{h(x,A)} [h(x,A) - \eta]\frac{\partial \sigma(x,\eta)}{\partial x}d\eta. \tag{29}$$

The magnitude of this force depends on the cross-sectional variation for a constant depth. Note that (i) this approach is underpinned by the hypothesis of gradual variation in flow variables and bed geometry and (ii) the streamwise gradient of the width is central to the accurate computation of the total pressure.

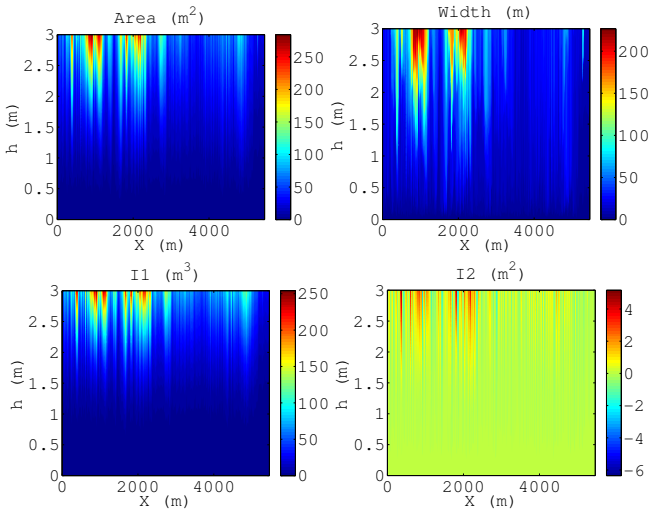

Figure 12: Dependence of channel area A, width b, pressure force terms I_1 and I_2 on the streamwise coordinate x and flow depth h.

In Eq. (26), the one-dimensional friction slope term required to close the model is taken in the form of the Darcy-Weisbach friction law

$$S_f = \frac{f}{8g}\frac{|\bar{v}|\bar{v}}{R_h}, \tag{30}$$

where f is the friction factor and R_h is the hydraulic radius of the channel. The last term Eq. (26) is the bed slope $S_0 \equiv -\partial y_b/\partial x$.

A numerical code was written in Matlab to automatically compute $A(x,h)$, $R_h(x,h)$, $b(x,h)$, $I_1(x,h)$ and $I_2(x,h)$ for a given digital elevation model (DEM) and path. Tabulated data were used in an in-house finite volume code [51], second-order accurate in space and time, as follows: unknowns A and Q at every time step were obtained by solving for Eq. (23)-Eq. (30); a bidimensional searching algorithm was then employed to obtain the value of h associated with A; next, the terms $I_1(x,h)$, $I_1(x,h)$ and $R_h(x,h)$ were updated using quadratic interpolation.

Geometrical inputs give us useful information about the uniformity of the river channel. For instance, on inspection of the channel area A, width b and pressure force terms, I_1 and I_2, for a fixed water flow depth h along the streamwise coordinate x, see Figure (12), it is readily observed that b and A remain nearly constant over $3 \leq x \leq 4.5$ km, whilst there are substantial variations in the upstream reach for $x \leq 3$ km. I_1 and I_2 exhibit a similar trend as well as other variables such as R_h (not shown here for brevity). The channel in the lower reach indeed corresponds to a narrow, deep, confined, and, entrenched single thread stream with steep, cascading, step/pool features and low sinuosity [52]. Conversely, the upper reach is a braided channel with frequently spaced scour/depositional bed forms. The complex stream pattern found upstream also exhibits numerous expansions and contractions, as seen in Figure (12) with the width variations, which are influenced by gravel pit and anthropogenic structures.

Taking into account the previous considerations, all of the terms in Eq. (23)-Eq. (30) were included in the

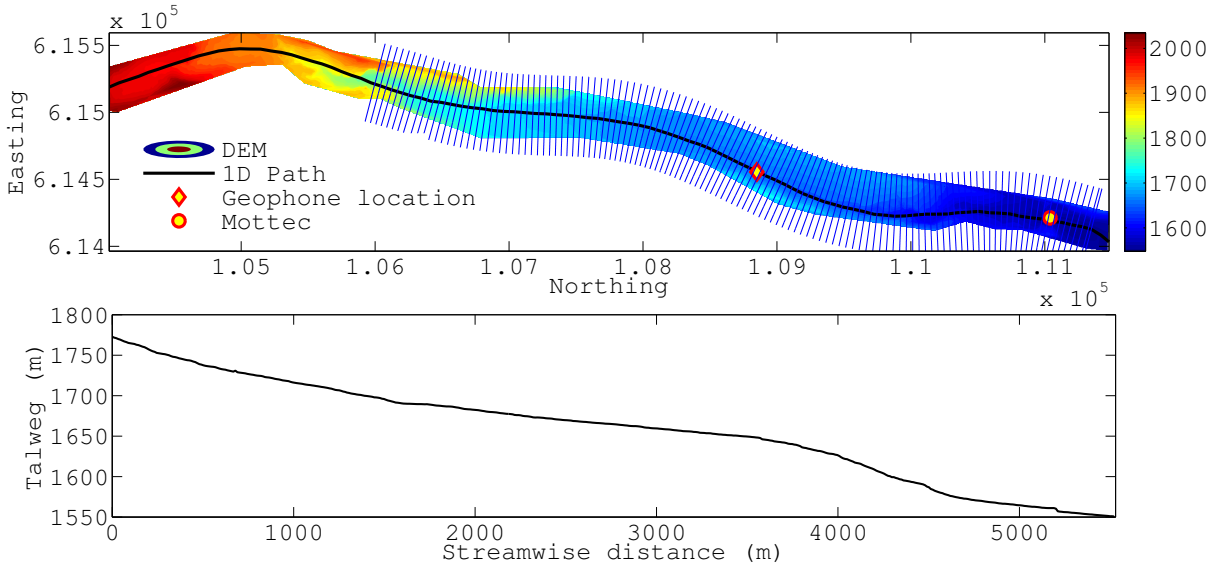

Figure 11: Digital elevation model of the study site (top) and talweg profile along northing (bottom). Blue lines represent the cross sections employed in the simulations (only 1 of every 5 are shown for the sake of clarity).

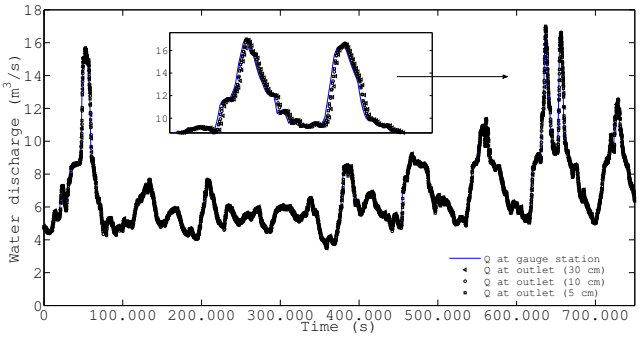

Figure 13: Comparison between inlet and outlet hydrographs for several grain sizes in Ferguson's equation [53; 54].

simulations. In doing so, their relative importance can be evaluated *a posteriori* to discuss further simplifications.

4.2 Unsteady simulation of circadian water discharge variations

Unsteady numerical results were obtained for a synoptic hydrograph measured at the Zinal gauge station (equipped with geophones to record bed load transport rates). The water flow discharge was set as an upstream boundary condition placed at this station. The inlet cross-section area was determined to impose a critical Froude number, i.e. A was given by the solution to the equation $Q = A^{3/2}\sqrt{g/b}$. The characteristic variable extrapolation method was employed at the outlet.

The sensitivity of the numerical results to grain size was evaluated using Ferguson's friction factor [53], which is particularly well suited for uniform regimes in gravel-bed rivers with constant cross section [54]. Figure (13) shows the outlet hydrograph obtained for a given inlet discharge (blue solid line) and characteristic grain sizes of $d_{84} = 5$, 10 and 30 cm. Surprisingly the outlet hydrograph preserves the same shape as that fixed at the inlet regardless of the diameter d_{84}. In a long temporal scale the inlet and outlet hydrographs nearly collapse. Looking into the details, we found out a small delay between them, see the inset of Figure (13), that amounts to a different lag time ranging from 473 s ($d_{84} = 5$ cm) to 931 s ($d_{84} = 30$ cm). An additional numerical simulation was performed using the Colebrook-White equation [55] with $d_{84} = 10$ cm. It agreed very well with the previous one, showing a lag time of about 720 s.

Field works were done on 14th October 2012 to measure the velocity field *in situ*. It was measured for moderate water discharges between 2 and 8 m^3/s at five points along the reach upstream of the geophones station. On average, the standard deviation of the mean velocity considered at each cross section was quite high (typically 0.8 m/s) compared to the mean flow velocity (approximately 2.7 m/s). This could be interpreted as the occurrence of non-uniform velocity profiles in the cross section and unsteady turbulent spots. The best agreement between prediction and mean experimental values was found with grain diameter values of about 10 cm. Maximum discrepancies were lower than 30 % when computing f using Colebrook-White's equation or Ferguson's law.

Previous results have important consequences for the hydraulic modelling of mountain rivers as it sets the validity of the kinematic wave approximation [56] and frictional laws in non-uniform quasi-steady regimes. We postulate that the propagation of a hydrograph wave form in mountain rivers can be computed as the solution to the first order wave equation (the so-called kinematic wave equation)

$$\frac{\partial Q}{\partial t} + c\frac{\partial Q}{\partial x} = 0\,, \tag{31}$$

where the wave speed c has to be estimated for a particular river reach and flow conditions. In addition, taking into account that the characteristic period of 24 h associated with circadian oscillations is much longer than the characteristic lag time of about 15 min for a reach of 2 km length, one can further assume a local quasi-steady regime. So, the water flow depth and the velocity corresponding to a given discharge Q can be obtained from the steady state solution of the momentum balance equation neglecting the gradients of Q, i.e. solving for

$$\bar{v}\frac{\partial \bar{v}}{\partial x} = g\left(S_0 - \frac{\partial h}{\partial x}\right) - \frac{f}{8}\frac{|\bar{v}|\bar{v}}{R_h}\,, \tag{32}$$

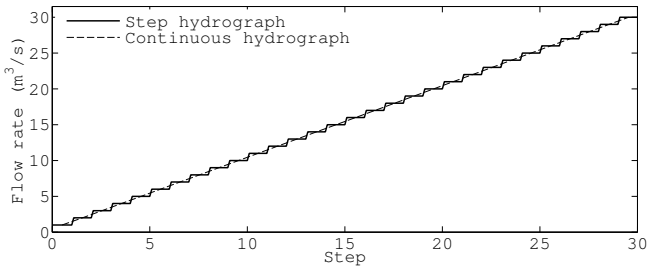

Figure 14: Step hydrograph imposed as boundary condition at the inlet. Results from step computations can be employed to mimic a continuous increase of the flow rate according to § 4.2.

in which [50]

$$\frac{\partial h}{\partial x} = \frac{1}{A}\left(\frac{\partial I_1}{\partial x} - I_2\right) . \tag{33}$$

Note that the spatial variations of the velocity $\bar{v}$ and flow depth h induced by cross section variations in non-uniform channels may play as important role as the bed slope S_0 and the bottom friction as will be shown in the next section.

4.3 Steady state computations

Steady state numerical simulations were performed for a realistic range of water discharges from 1 to 30 m^3/s. The water discharge was fixed as an upstream boundary condition together with the area corresponding to a critical Froude number, similarly to the unsteady case. A sensitivity study, not shown here for the sake of the brevity, has proven that the numerical solution taken a few meters downstream of the inflow is insensitive to the water depth at the inlet. Hence, in the present case, flow hydrodynamics only depend on the river geometry, frictional resistance and discharge.

Numerical simulations were performed sequentially to save computational time. To this end the step hydrogram shown in Figure (14) was set at the inlet. A constant value of the discharge was maintained during the integration of Eq. (23)-Eq. (30) until a steady state is reached throughout the whole computational domain. Subsequently, it was monotonously increased by steps of 1 m^3/s ensuring steady state solutions at every discharge. The numerical solution obviously satisfies the steady state equation, Eq. (32)-Eq. (33), and allow us to evaluate the relative importance of the bed slope and momentum transfer to the bed (i.e. hydraulic resistance in uniform channels) relative to the terms, which can be interpreted as local resistance arising from the non-uniformity of the channel geometry.

In this context, we sought to evaluate the local energy loss caused by the non-uniformity of the river channel, denoted hereafter by S_g and defined as the deviation of the friction slope S_f with respect to the bed slope S_0:

$$S_g \equiv \frac{\bar{v}}{g}\frac{\partial \bar{v}}{\partial x} + \frac{\partial h}{\partial x} = S_0 - S_f . \tag{34}$$

Figure (15) shows the percentage value of the local head loss S_g scaled by S_0 obtained in the numerical simulations as a function of the water discharge. To make the description easier, we plotted the average value in the whole river. The average head losses induced by streamwise variations in the hydraulic variables amount

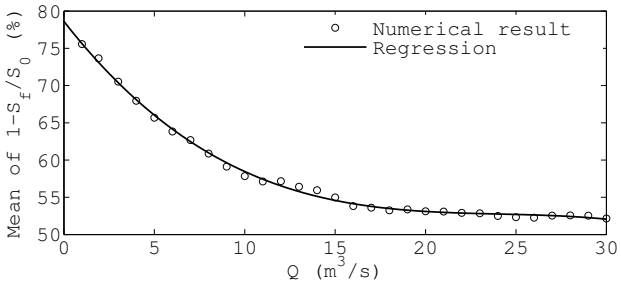

Figure 15: Relative local head loss S_g/S_0.

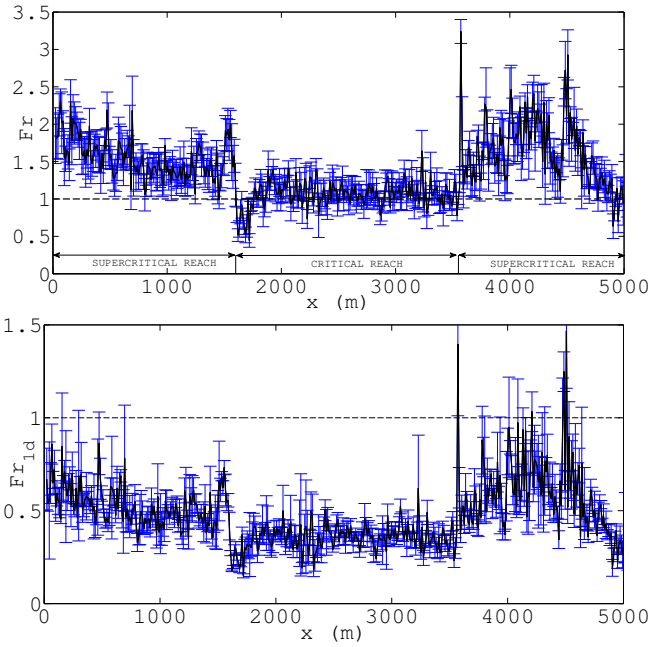

Figure 16: Mean value (black solid line) and standard deviation of the cross section (top) and 1d (bottom) Froude number for water discharges between 1 and 30 m^3/s.

to more than fifty percent of the bed slope, with a maximum reached at low stages at which average head loss approaches 80%. It monotonously decreases as the flow discharge raises, attaining a minimum asymptotic value (which is above 50%) for flow discharges exceeding 20 m^3/s. This result highlights the clear hydraulic control exerted by the river channel, which turns out to be significant at the lowest flow rates. This feature has to be accounted for in the hydraulic modelling if the objective is to be accurate.

The Froude number $Fr \equiv Q/\sqrt{A^3 g/b}$ follows a well-defined trend at all flow discharges, as shown in Figure (16). Three hydraulic regimes are visible. The flow is supercritical upstream ($x < 1600$ m), becomes nearly critical approximately along the next 2 km and finally returns to the supercritical regime further downstream ($x > 3550$ m). The average value of the ratio between the standard deviation and the mean Froude number is lower than 14% when Q ranges from 1 to 30 m^3/s at any x. A similar behaviour is observed if we use the one-dimensional definition of the Froude number $Fr_{1d} = \bar{v}/\sqrt{gh}$ (whereas its value differs markedly from the cross-sectionally averaged one Fr).

This remarkable result demonstrates that the solution exhibits Froude similarity at leading order. This property simplifies and tremendously speeds up the computation of flow depth and velocity for a given flow discharge. As a matter of fact, assuming that the Froude

number Fr^* is known at a given location x, for instance calculating it from field data or by means of numerical simulations just at one discharge Q^*, the flow depth h at an arbitrary discharge Q can be obtained by solving the equation

$$\frac{A^3}{b}(x,h) = \frac{1}{g}\left(\frac{Q}{Fr^*}\right)^2 . \tag{35}$$

Alternatively, one can solve h and $\bar{v}$ along the thalweg from

$$\frac{\bar{v}}{\sqrt{g\,h}} = Fr^*_{1d} \quad \text{with} \quad \bar{v} = \frac{Q}{A(x,h)} . \tag{36}$$

5 Concluding remarks

Our project (which started five years ago) has made steady progress, with some interesting achievements regarding the stochastic modelling of sediment transport and the numerical simulations. Here we summarize the main findings, speak of the future work, and highlight some of limitations in our current framework.

5.1 Stochastic model of sediment transport

Our Markov-process-based approach has addressed at least two issues in the list of problems enumerated in § 2:

- Existence of large non-Gaussian fluctuations and sediment rating curve: in the absence of collective entrainment ($\mu = 0$), the fluctuations of N are Poissonian, which leads to a rather simple macroscopic behaviour [9]. In contrast, for $\mu > 0$, fluctuations are non-Poissonian and may vary significantly over time, affecting the macroscopic behaviour by the growth of spatial correlations, which reflects local increases in the particle activity. Even for steady uniform flow conditions (with no bed forms), the variance of the particle flux may become very large. For time-dependent flow conditions and especially when bed forms migrate, the expected behaviour of fluctuations is quite complicated. The Langevin equation associated with the Fokker-Planck equation Eq. (9) reveals that the noise structure, characterized by a square multiplicative noise term, differs significantly from the white noise term used by Jerolmack and Mohrig [19] to model the stochastic development of bed forms [10]. Altogether, this provides us with little reason to believe that in real flow conditions, marked by time dependence and bed form migration, one can obtain consistent time averages of the particle activity and sediment transport rates. In our opinion, this explains the failure in both the laboratory [45] and the field [57; 58] to arrive at robust estimates of transport rates when the sampling rate is changed. As a consequence, the idea of a unique bed load rating curve seems dubious.

- Existence of long correlation lengths and bed forms: when collective entrainment occurs ($\mu > 0$), the spatial correlation function is nonzero and decays exponentially; the detail is given in [10]. From the combined action of the water stream (through D_u) and sediment transport (through the deposition and entrainment rate difference κ), emerges the correlation length scale $\ell_c = \sqrt{D_u/\kappa}$. Similarly, the autocorrelation time of the number of moving particles is $t_c = 1/\kappa$ can be quite long (compared to flow characteristic times). Collective entrainment is consistent with the incipient phase of dune formation: for $\mu > 0$, there are areas characterized by high correlations in the particle activity, whose strength is dictated by the ratio μ/κ. This is likely to cause nonhomogeneous sediment transport, which in turn promotes bed form development. From this perspective, the initiation of bed structure is the consequence of collective entrainment. The subsequent development of bed patterns is, however, beyond the scope of our analytical application as it requires calculating the coupling between the stream and topography, and more specifically the effects of turbulence on particle entrainment.

Another particularly interesting result is related to the difference between the definition of the sediment transport rate at the micro- and macroscales. We come to conclusions similar to those drawn by Furbish *et al.* [31] about the form that the particle flux should take. The governing equation of the particle activity Eq. (21), derived from the microscopic description of particle transport, matches the Exner equation Eq. (6) provided that (i) the particle transport rate is defined at the macroscopic scale as

$$\bar{q}_s = \mathcal{Q}(x,t) = \langle\gamma\rangle\bar{u}_s - \frac{\partial}{\partial x}(D_u\langle\gamma\rangle), \tag{37}$$

and (ii) the term $\partial_t\langle\gamma\rangle$ is negligible relative to entrainment and deposition rates. The latter assumption is well-established [48]. This definition of $\bar{q}_s$ differs from the local definition Eq. (3). The interpretation of the present stochastic analysis closely follows those obtained by Furbish *et al.*: at the macroscopic scale, diffusive effects are present in the Exner equation, which modulate, to a varying degree, the advection term. The significance of this modulation can be estimated using a dimensionless Péclet number [10].

In the coming years, the main tasks concern the extension of the model to deal with non-uniform flow conditions, which involves studying the difficult question of the coupling between bed topography, turbulence, and particle entrainment. Two stumbling blocks remain the definition of the particle flux and the dependence of the entrainment and deposition parameter under time-dependent flow conditions.

In the current framework, there are different possibilities of modelling the particle flux between cells. Here, we have presented one variant based on the decomposition of the particle flux into advection and diffusion [10]. Thanks to a Poisson transform, we can simulate the probability distribution of the particle activity in a continuous probably space (referred to the a-space above) and obtain results that should be valid independently of the cell size. The drawback of this formulation is the difficulty to get the back-transformation of the particle activity probability. So, for the moment, we can calculate the moments of the number of moving particles N (or particle activity γ), but the full probability distribution (in the physical space) is more difficult to calculate.

Another possibility is to use a system-size expansion of the discrete probabilities [7]. In that case, the governing equation of the particle activity can be approximated as a Fokker-Planck equation (but directly in the physical space contrary to the previous formulation). The advantage is that the formalism is simpler, with no recourse to transform. The disadvantage is that this approximation holds true only for sufficiently large cell sizes.

5.2 Water flow

A one-dimensional, cross-sectional-averaged Saint-Venant model has been adopted in order to analyse the hydraulics of a mountain river (La Navisence, Swiss Alps) at moderate water flow discharges in which bed load transport is weak.

The detailed study of circadian variations of the water discharge has shown that the flow regime is quasi-steady to leading order. The propagation of an arbitrary discharge wave along the river can be readily computed from the one-dimensional wave equation Eq. (31) in which the wave speed c is fixed by the bed roughness or grain size d_{85} and by the main channel geometry.

Strikingly, the thorough analysis of the steady state solution to the cross-sectionally averaged Saint-Venant equations Eq. (23)-Eq. (30) for a wide range of water flow discharges have proven the existence of Froude similarity in the flow processes. This feature is of paramount importance to the subsequent developments as it allows us to reconstruct the hydraulic conditions in a river section at any state Q by simply solving an algebraical system of equations, given by Eq. (35)-Eq. (36), where the input parameters are the channel bathymetry and the Froude number Fr^* (or Fr^*_{1d}) at some discharge Q^*. The Froude number can be measured experimentally or computed from numerical simulations.

The value of the Froude number depends greatly on the definition used: it can be computed using the cross-section (Fr) or the flow variables along the thalweg (Fr_{1d}). As shown by Figure (16), the differences between Fr and Fr_{1d} result from the channel geometry influence on the fluvial hydraulics since local head losses S_g are of the same order of magnitude as the bed slope S_0, as shown by Figure (15).

Acknowledgment

The work summarized here was supported by the Swiss National Science Foundation under grants No. 200021-129538 (a project called "The Stochastic Torrent: stochastic model for bed load transport on steep slope") and No. 200021-105193/1 (a project called "Transient free-surface flows of concentrated suspensions–Application to geophysical flows," funded by an R'Equip grant). P.B. thanks CEACTierra (University of Jaén) for partial financial support. The project is part of a longer programme spanning several years and which has benefited from feedback and many discussions. We are indebted to our colleagues Eric Travaglini from CREALP (Sion, Switzerland), Prof. Anthony Davison (EPFL), and Dr. Philippe Frey (IRSTEA, France). Most of the data presented here was obtained by Tobias Böhm during his thesis.

References

[1] V. Koulinski, *Étude de la formation d'un lit torrentiel par confrontation d'essais sur modèle réduit et d'observations sur le terrain.* Ph.D. Thesis, Grenoble, 1993.

[2] H. A. Einstein, "The bed-load function for sediment transportation in open channel flows," Technical Report No. 1026, United States Department of Agriculture, 1950.

[3] R. A. Bagnold, "An approach to the sediment transport problem from general physics," professional paper 422-I, United States Geological Survey, 1966.

[4] F. Comiti and L. Mao, "Recent advances in the dynamics of steep channels," in *Gravel-bed rivers: Processes, tools, environments* (M. Church, P. M. Baron, and A. G. Roy, eds.), pp. 351–377, 2012.

[5] G. K. Gilbert and E. C. Murphy, "The transportation of debris by running water," US Government Printing Office, 1914.

[6] M. P. du Boys, "Etudes du régime du Rhône et de l'action exercée par les eaux sur un lit à fond de graviers indéfiniment affouillable," *Annales des Ponts et Chaussées*, Série 5, No. 18, pp. 141–95, 1879.

[7] C. Ancey, "Stochastic approximation of the Exner equation under lower-regime conditions," *J. Geophys. Res.*, vol. 115, p. F00A11, 2010.

[8] F. Ballio, V. Nikora, and S. E. Coleman, "On the definition of solid discharge in hydro-environment research and applications," *J. Hydraul. Res.*, vol. 52, pp. 173–184, 2014.

[9] C. Ancey, A. C. Davison, T. Böhm, M. Jodeau, and P. Frey, "Entrainment and motion of coarse particles in a shallow water stream down a steep slope," *J. Fluid Mech.*, vol. 595, pp. 83–114, 2008.

[10] C. Ancey and J. Heyman, "A microstructural approach to bed load transport: mean behaviour and fluctuations of particle transport rates," *J. Fluid Mech.*, vol. 744, pp. 129–168, 2014.

[11] S. A. Schumm, *River Variability and Complexity.* Cambridge: Cambridge University Press, 2005.

[12] M. Church, "Bed material transport and the morphology of alluvial river channels," *Annu. Rev. Earth. Planet. Sci.*, vol. 34, pp. 325–354, 2006.

[13] S. E. Coleman and V. I. Nikora, "Fluvial dunes: initiation, characterization, flow structure," *Earth Surf. Process. Landforms*, vol. 36, pp. 39–57, 2011.

[14] D. Rickenmann, "Hyperconcentrated flow and sediment transport at steep slopes," *J. Hydraul. Eng.*, vol. 117, pp. 1419–1439, 1992.

[15] G. Seminara, "Fluvial sedimentary patterns," *Annu. Rev. Fluid Mech.*, vol. 42, pp. 43–66, 2010.

[16] M. Colombini and A. Stocchino, "Ripple and dune formation in rivers," *J. Fluid Mech.*, vol. 673, pp. 121–131, 2011.

[17] Y. Niño, A. Atala, M. Barahona, and D. Aracena, "Discrete particle model for analyzing bed form development," *J. Hydraul. Eng.*, vol. 128, pp. 381–389, 2002.

[18] F. Sagués, J. M. Sancho, and J. García-Ojalvo, "Spatiotemporal order out of noise," *Rev. Mod. Phys.*, vol. 79, pp. 829–882, 2007.

[19] D. Jerolmack and D. Mohrig, "A unified model for subaqueous bed form dynamics," *Water Resour. Res.*, vol. 41, W12421, 2005.

[20] Y. Shimizu, S. Giri, S. Yamaguchi, and J. Nelson, "Numerical simulation of dune-flat bed transition and stage-discharge relationship with hysteresis effect," *Water Resour. Res.*, vol. 45, W04429, 2009.

[21] R. A. Kuhnle and J. B. Southard, "Bed load transport fluctuations in a gravel bed laboratory channel," *Water Resour. Res.*, vol. 24, pp. 247–260, 1988.

[22] B. Gomez, R. L. Naff, and D. W. Hubbell, "Temporal variations in bed load transport rates associated with the migration of bed forms," *Earth Surf. Process. Landforms*, vol. 14, pp. 135–156, 1989.

[23] T. B. Hoey, "Temporal variations in bed load transport rates and sediment storage in gravel-bed rivers," *Prog. Phys. Geog.*, vol. 16, pp. 319–338, 1992.

[24] M. Esfeld, *Holism in Philosophy of Mind and Philosophy of Physics*, vol. 298. Springer, 2001.

[25] B. C. Eaton and M. A. Hassan, "Scale-dependent interactions between wood and channel dynamics: Modeling jam formation and sediment storage in gravel-bed streams," *J. Geophys. Res.*, vol. 118, pp. 2500–2508, 2013.

[26] M. Tal and C. Paola, "Dynamic single-thread channels maintained by the interaction of flow and vegetation," *Geology*, vol. 35, pp. 347–350, 2007.

[27] M. H. García, "Sediment transport and morphodynamics," in *Sedimentation Engineering* (M. H. García, ed.), vol. ASCE Manuals and Reports on Engineering Practice 110, pp. 21–164, Reston: American Society of Civil Engineers, 2007.

[28] C. Parés, "Numerical methods for nonconservative hyperbolic systems: a theoretical framework," *SIAM J. Numer. Anal.*, vol. 44, pp. 300–321, 2006.

[29] G. Fasolato, P. Ronco, E. J. Langendoen, and G. Di Silvio, "Validity of uniform flow hypothesis in one-dimensional morphodynamic models," *J. Hydraul. Eng.*, vol. 137, pp. 183–195, 2011.

[30] C. Paola and V. R. Voller, "A generalized Exner equation for sediment mass balance," *J. Geophys. Res.*, vol. 110, F04014, 2005.

[31] D. J. Furbish, P. K. Haff, J. C. Roseberry, and M. W. Schmeeckle, "A probabilistic description of the bed load sediment flux: 1. Theory," *J. Geophys. Res.*, vol. 117, F03031, 2012.

[32] A. Recking, P. Frey, A. Paquier, P. Belleudy, and J. Y. Champagne, "Feedback between bed load transport and flow resistance in gravel and cobble bed rivers," *Water Resour. Res.*, vol. 44, W05412, 2008.

[33] D. T. Gillespie, *Markov Processes: An Introduction for Physical Scientists*. San Diego: Academic Press, 1992.

[34] C. W. Gardiner, *Handbook of Stochastic Methods*. Berlin: Springer Verlag, 1983.

[35] J. C. Cox, J. E. Ingersoll, and S. A. Ross, "A theory of the term structure of interest rates," *Econometrica*, vol. 53, pp. 385–407, 1985.

[36] S. M. Iacus, *Simulation and Inference for Stochastic Differential Equations*. New York: Springer, 2008.

[37] E. Lajeunesse, L. Malverti, and F. Charru, "Bed load transport in turbulent flow at the grain scale: Experiments and modeling," *J. Geophys. Res.*, vol. 115, F04001, 2010.

[38] R. L. Martin, D. J. Jerolmack, and R. Schumer, "The physical basis for anomalous diffusion in bed load transport," *J. Geophys. Res.*, vol. 117, F01018, 2012.

[39] D. J. Furbish and M. W. Schmeeckle, "A probabilistic derivation of the exponential-like distribution of bed load particle velocities," *Water Resour. Res.*, vol. 49, pp. 1537-1551, 2013.

[40] N. Fan, D. Zhong, B. Wu, E. Foufoula-Georgiou, and M. Guala, "A mechanistic-stochastic formulation of bed load particle motions: From individual particle forces to the Fokker-Planck equation under low transport rates," *J. Geophys. Res.: Earth Surface*, vol. 119, pp. 464-482, 2014.

[41] J. C. Roseberry, M. W. Schmeeckle, and D. J. Furbish, "A probabilistic description of the bed load sediment flux: 2. Particle activity and motions," *J. Geophys. Res.*, vol. 117, F03032, 2012.

[42] A. Hamamori, "A theoretical investigation on the fluctuations of bed load transport," Tech. Rep. Report R4, Delft Hydraulics Laboratory, 1962.

[43] J. M. Turowski, "Probability distributions of bed load transport rates: A new derivation and comparison with field data," *Water Resour. Res.*, vol. 46, W08501, 2010.

[44] A. Radice, "Use of the Lorenz curve to quantify statistical nonuniformity of sediment transport rate," *J. Hydraul. Eng.*, vol. 135, pp. 320–326, 2009.

[45] A. Singh, K. Fienberg, D. J. Jerolmack, J. Marr, and E. Foufoula-Georgiou, "Experimental evidence for statistical scaling and intermittency in sediment transport rates," *J. Geophys. Res.*, vol. 114, doi: 2007JF000963, 2009.

[46] G. Parker, C. Paola, and S. Leclair, "Probabilistic Exner sediment continuity equation for mixtures with no active layer," *J. Hydraul. Eng.*, vol. 126, pp. 818–826, 2000.

[47] Z. Cao, R. Day, and S. Egashira, "Coupled and decoupled numerical modeling of flow and morphological evolution in alluvial rivers," *J. Hydraul. Eng.*, vol. 128, pp. 306–321, 2002.

[48] Y. Cui, G. Parker, T. E. Lisle, J. E. Pizzuto, and A. M. Dodd, "More on the evolution of bed material waves in alluvial rivers," *Earth Surf. Process. Landforms*, vol. 30, pp. 107–114, 2005.

[49] R. Hoyle, *Pattern Formation*. Cambridge: Cambridge University Press, 2006.

[50] J. A. Cunge, F. M. Holly, and A. Verwey, *Practical aspects of computational river hydraulics*. Pitman: London, UK, 1980.

[51] P. Bohorquez and S. E. Darby, "The use of one- and two-dimensional hydraulic modelling to reconstruct a glacial outburst flood in a steep Alpine valley," *J. Hydrol.*, vol. 361, pp. 240–261, 2008.

[52] D. L. Rosgen, "A classification of natural rivers," *Catena*, vol. 22, pp. 169–199, 1994.

[53] R. I. Ferguson, "Flow resistance equations for gravel- and boulder-bed streams," *Water Resour. Res.*, vol. 43, W05427, 2007.

[54] D. Rickenmann and A. Recking, "Evaluation of flow resistance in gravel-bed rivers through a large field data set," *Water Resour. Res.*, vol. 47, W07538, 2011.

[55] C. F. Colebrook and C. M. White, "Experiments with fluid friction in roughened pipes," *Proc. R. Soc. London ser. A*, vol. 161, No. 906, pp. 367–381, 1937.

[56] M. J. Lighthill and G. B. Whitham, "On kinematic waves. I. Flood movement in long rivers," *Proc. R. Soc. London ser. A*, vol. 229, pp. 281–316, 1955.

[57] K. Bunte and S. Abt, "Effect of sampling time on measured gravel bed load transport rates in a coarse-bedded stream," *Water Resour. Res.*, vol. 41, W11405, 2005.

[58] A. Recking, F. Liébault, C. Peteuil, and T. Jolimet, "Testing bed load transport equations with consideration of time scales," *Earth Surf. Process. Landforms*, vol. 37, pp. 774–789, 2012.